

# Assembly of Nanometer-Sized Hollow Sphere Colloidal Crystals for Applications as Tunable Photonic Materials

Chia-Hua Hsieh, Fang-Tzu Lin, Kun-Yi Andrew Lin, Shang-Yu Hsieh, Yi-Ting Chen, Hui-Ping Tsai,\* Chieh-Hsuan Lu, and Hongta Yang\*



Cite This: *ACS Appl. Nano Mater.* 2022, 5, 15855–15864



Read Online

ACCESS |

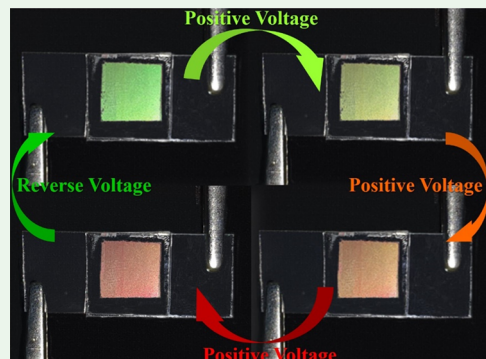
Metrics & More

Article Recommendations

Supporting Information

**ABSTRACT:** Electrically responsive photonic crystals, capable of transforming crystal structures and changing intrinsic structural colors in response to external electrical energies, can serve as optically active components for promising technological applications. Unfortunately, the deformation of inverse opal photonic crystals generally weakens the structural stability and leads to poor color tuning repeatability, while most color-tunable colloidal photonic crystals suffer from low color saturation as a result of small refractive index difference between the colloids and matrices. Inspired by cephalopod skins, nanometer-sized hollow silica sphere/poly(3,4-ethylenedioxythiophene)-polystyrene sulfonate photonic crystals are self-assembled using a scalable coating technique. The as-engineered photonic crystals exhibit a conspicuous structural color that is tunable on demand by applying varied voltages. Importantly, their appearance and expanded crystalline lattice can be maintained without any electric field under ambient conditions and simultaneously recovered by applying an oxidation potential. The reversibility and the dependence of hollow sphere size and thickness on electrochromic behaviors are also investigated in this study.

**KEYWORDS:** cephalopod skins, hollow spheres, photonic crystals, self-assembly, reversibility



## INTRODUCTION

Photonic crystals, materials with a periodic variation in the refractive index, possess an energy gap to forbid the propagation of electromagnetic waves with a certain energy.<sup>1,2</sup> The photonic band gap materials thereby reflect incident light within narrow bands of wavelengths, making them a fecund test-bed for manipulating light flow. In contrast to the visual appearance of common colorants, such as pigments and dyes, the nonbleachable structural colors arising from Bragg optical diffraction can be tuned throughout the entire visible spectrum by adjusting the spatial arrangement and effective refractive index of photonic crystals. To tune the structural colors on demand, diverse stimuli-responsive mechanisms are coupled with the photonic structures to convert external stimuli into optical responses either permanently or reversibly.<sup>3–6</sup> Among these stimuli, the electrical stimulus has drawn plenty of interest due to its low operational current/voltage, high electrical tunability, and rapid response time. Accordingly, electrically responsive photonic crystals can be a promising candidate for various practical applications, including displays, anticounterfeiting materials, army camouflage, security devices, optical filters, chemical/biological sensors, and interactive wearable devices.<sup>7–14</sup>

Given such flamboyant potential applications, electrophoretic forces have been adopted to modify the photonic band gaps of crystalline colloidal arrays in concentrated

colloidal suspensions.<sup>15–18</sup> Charged monodisperse colloids are spontaneously organized into photonic structures owing to the electrostatic repulsions among the colloids. Upon introducing an electric field, the charged colloids tend to move toward the oppositely charged electrode, and thus their intercolloid distances decrease along a single direction near this electrode. As a result, the compression of the colloidal lattice triggered by the electrokinetic forces leads to a blue shift of its photonic band gap and a corresponding color change. The optimized reflection wavelength shift can therefore be determined by varying the electric field intensity. Nevertheless, the reflection intensity falls seriously under a high voltage, resulting from the absence of long-range lattice periodicity.<sup>19,20</sup> For that reason, the electrophoretic force-induced colloidal arrays suffer from incomplete photonic band gaps and low optical saturation performances. Other common drawbacks concern their inevitable hysteresis and low cycle rates, restricting their implementation in real applications.<sup>21</sup>

Received: September 16, 2022

Accepted: September 22, 2022

Published: October 7, 2022



To tackle these challenges, a variety of electrically responsive polymers accompanied by appropriate conductive electrolytes have been extensively exploited to develop color-tunable photonic crystals, which are triggered by reversible reduction/oxidation processes.<sup>22–25</sup> External electrical stimuli, such as electric field, can be applied to induce localized charge variations on the active moieties of polymer chains by changing their oxidation states. To minimize electrostatic repulsions between the ionized moieties, the polymer chains undergo structural reorganizations, and hence electrolyte molecules are driven into the polymeric matrix to neutralize their charges. In addition to a change of effective refractive index, the process brings about a larger crystalline lattice spacing and a shift of the photonic band gap as well. Although these electrically responsive colloidal photonic crystals present reversible and stable color changes with high response speeds, only low reflection intensities are allowed due to the small refractive index contrasts between colloids and polymers.<sup>26</sup> In addition, restricted by the intrinsic cross-linking degree and porosity of the polymeric matrix, the color transform range is confined. By contrast, inverse opal photonic crystals express less resistance against anisotropic expansion/contraction of the photonic lattice, thereby delivering a color transform across the entire visible spectrum.<sup>27</sup> In spite of that, the deformation of inverse opal photonic crystals weakens the structure stability and leads to poor color tuning repeatability. Moreover, their color saturations are not significantly enhanced in view of the small refractive index contrasts between electrolytes and polymers. Alternatively, electrically responsive hydrogels are presented and proposed to improve the cyclic stability in repeated usage.<sup>28,29</sup> The inverse opal hydrogels exhibit switchable colors in the visible region in response to external electrical stimuli. Unfortunately, the system possesses a pH gradient perpendicular to the electrode, generating a nonuniform volume change of the macroporous hydrogel.<sup>30</sup> Different regions of the hydrogel therefore feature different colors, accompanied by a very long switching time. As a consequence, electrochromic photonic crystals allowing fast, uniform, and reversible color tuning over a wide range with low voltages remain an unmet yet urgent need.

Over more than 400 million years of natural selection, living organisms have evolved diverse features and favorable lifestyles to adapt to their current environments. For instance, banded demoiselles, jewel beetles, gold beetles, blue morpho butterflies, Madagascan sunset moths, and orchid bees have brought forward a wide variety of photonic structures to reflect incident light.<sup>31,32</sup> Body colorations allow the insects to provide camouflage against predators on the hunt, warn predators of toxicity, increase visibility to potential mates, or create a dynamic form of information. Some specific cephalopods, as the most intelligent invertebrate, can even tune structural colors across the entire visible spectrum without the loss of color fidelity.<sup>33–35</sup> The adaptive coloration is enabled by modulating the geometry and extracellular spacing of Bragg stack hollow architectures within dermal iridophores in their soft and fixable skins. The next generation of electrically responsive color-changing materials can benefit from the lessons through using nanometer-sized hollow particles to fabricate photonic crystals.

Apart from that, large-scale manufacturing of photonic crystals still remains a technical challenge. In spite of the fact that a large variety of lithography-based technologies have been developed to overcome the challenge, the methodologies are

restricted to complex operating processes, high operating costs, and requirements for sophisticated equipment.<sup>36</sup> Compared with the top-down approaches, spontaneous crystallization of monodisperse nanometer-sized colloids renders a relatively simple and inexpensive strategy to self-assemble large-scale photonic crystals. Unfortunately, most of the current bottom-up approaches, including magnetic/electric-field-assisted assembly, physical confinement, capillary-force-induced self-assembly, and gravitational sedimentation, are time-consuming and only favorable for laboratory-scale production.<sup>37,38</sup> To address the scale-up challenge, a roll-to-roll compatible shear-force-induced assembly technique has recently been developed to doctor-blade-coat three-dimensional colloidal crystals over large areas.<sup>39</sup> On account of its high-throughput coating rate, low coating material wastage, and wide range of coating materials, this approach can be suitable for industrial-scale mass production. In the following, the doctor-blade coating technique is utilized to self-assemble electrochromic photonic films composed of close-packed nanometer-sized hollow spherical colloids embedded in electrically responsive polymeric matrices inspired by the iridophore structure of cephalopods. The structural color of the as-designed photonic crystals has high color saturation, and the color can be real-time altered on demand by applying required voltages. The novel electrochromic photonic crystals are easily scalable, highly reversible, and mechanically robust, realizing perceivable monitoring by legible optical signals.

## EXPERIMENTAL SECTION

**Materials.** The chemicals employed to synthesize silica hollow spheres, including styrene monomers (99%) (Thermo Fisher Scientific Co.), sodium dodecyl sulfate ( $\geq 97\%$ ) (Merck KGaA Co., Germany), potassium persulfate ( $\geq 99\%$ ) (Thermo Fisher Scientific Co.), absolute ethanol ( $\geq 99\%$ ) (ECHO Chemical Co., Ltd., Taiwan), tetraethyl orthosilicate ( $\geq 98\%$ ) (Merck KGaA Co., Germany), and ammonium hydroxide ( $\geq 28\%$ ) (Thermo Fisher Scientific Co.) are used as received, except styrene monomers. The styrene monomers are purified by distillation under vacuum before use. Deionized water with a resistivity of  $\geq 18.4 \text{ M}\Omega \text{ cm}$  is obtained from a Milli-Q IQ 7003 ultrapure water system (Merck KGaA Co., Germany). Commercial poly(3,4-ethylenedioxythiophene)-poly(styrenesulfonate) aqueous solution (PEDOT:PSS, 1.3 wt %, conductive grade) (Merck KGaA Co., Germany), lithium perchlorate ( $\geq 99\%$ ) (Merck KGaA Co., Germany), and propylene carbonate ( $\geq 99\%$ ) (Merck KGaA Co., Germany) are of reagent grade and used without any purification.

**Preparation of Silica Hollow Sphere Suspensions.** Silica hollow spheres with tunable size and thickness are prepared using spherical polystyrene particles as templates.<sup>40,41</sup> First, monodisperse polystyrene spheres are synthesized via an emulsion polymerization method.<sup>42</sup> Droplets of the purified styrene monomer are emulsified with anionic sodium dodecyl sulfate in deionized water, in which negatively charged emulsions repel each other electrostatically from coagulating. The polymerization of the styrene monomer is carried out by adding potassium persulfate as an initiator at  $80^\circ\text{C}$  under a nitrogen atmosphere. After 24 h, the resulting polystyrene spheres are washed with absolute ethanol thrice by repeating dispersion/centrifugation cycles to eliminate any undesired chemicals and byproducts, where the rotational speed is set at 8000 rpm. Thereafter, the purified polystyrene spheres are coated with silica through a modified Stöber method.<sup>43,44</sup> In

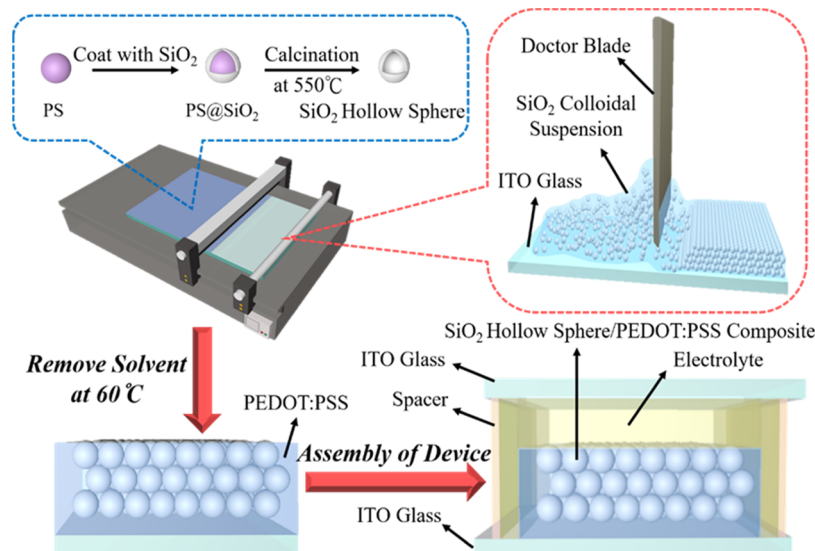


**Figure 1.** Schematic for the fabrication of a silica hollow sphere/PEDOT:PSS photonic crystal-based electrochromic device.

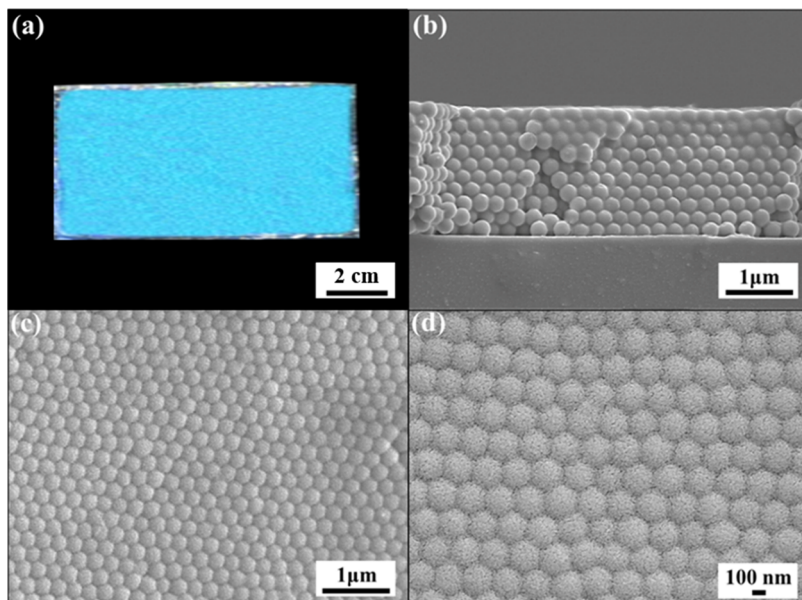


**Figure 2.** Silica hollow sphere/PEDOT:PSS photonic crystals fabricated by the doctor-blade coating technique. (a) Photographic image of the photonic crystals composed of close-packed 240 nm silica hollow spheres embedded in a PEDOT:PSS matrix. (b) Top-view SEM image, (c) cross-sectional SEM image, and (d) magnified cross-sectional SEM image of the sample in (a).

the sol–gel process, polystyrene spheres are dispersed in a mixture of tetraethyl orthosilicate, absolute ethanol, and deionized water under vigorous stirring, followed by rapidly injecting ammonium hydroxide into the mixture. The reaction is performed with a constant stirring speed of 500 rpm at 50 °C for 12 h. The as-synthesized polystyrene core/silica shell spheres are cleansed with absolute ethanol for another three dispersion/centrifugation cycles and then calcined at 550 °C in a furnace for 4 h. The polystyrene cores are with a thermal decomposition temperature ranging from 500 to 600 °C, suggesting that the templates cannot be completely removed under lower calcination temperatures.<sup>45,46</sup> By contrast, the as-fabricated silica hollow spheres are collapsed and even cannot remain mainly intact under higher calcination temperatures, resulting from the increase of Young's modulus. Finally, silica hollow spheres are collected and redispersed in a commercial

poly(3,4-ethylenedioxythiophene)–polystyrene sulfonate (PEDOT:PSS) solution.

**Fabrication of an Electrically Responsive Photonic Crystal-Based Electrochromic Device.** Silica hollow sphere/PEDOT:PSS photonic crystals are created by doctor-blade-coating the as-prepared silica colloidal suspension onto an indium tin oxide (ITO)-coated glass slide (Ruiling Optoelectronics Co., Ltd., Taiwan), which has been coated with a PEDOT:PSS wetting layer. The coating speed is maintained at 4 mm/min using a PFA-2010 automatic film applicator (Proyes International Co., Taiwan). In the coating procedure, a doctor blade is utilized to uniformly spread the suspension and to offer a unidirectional shear force for aligning the silica hollow spheres. The self-assembled composite is then solidified by complete evaporation of residual water at 40 °C for 3 h in a conventional oven. Afterward, a gel electrolyte

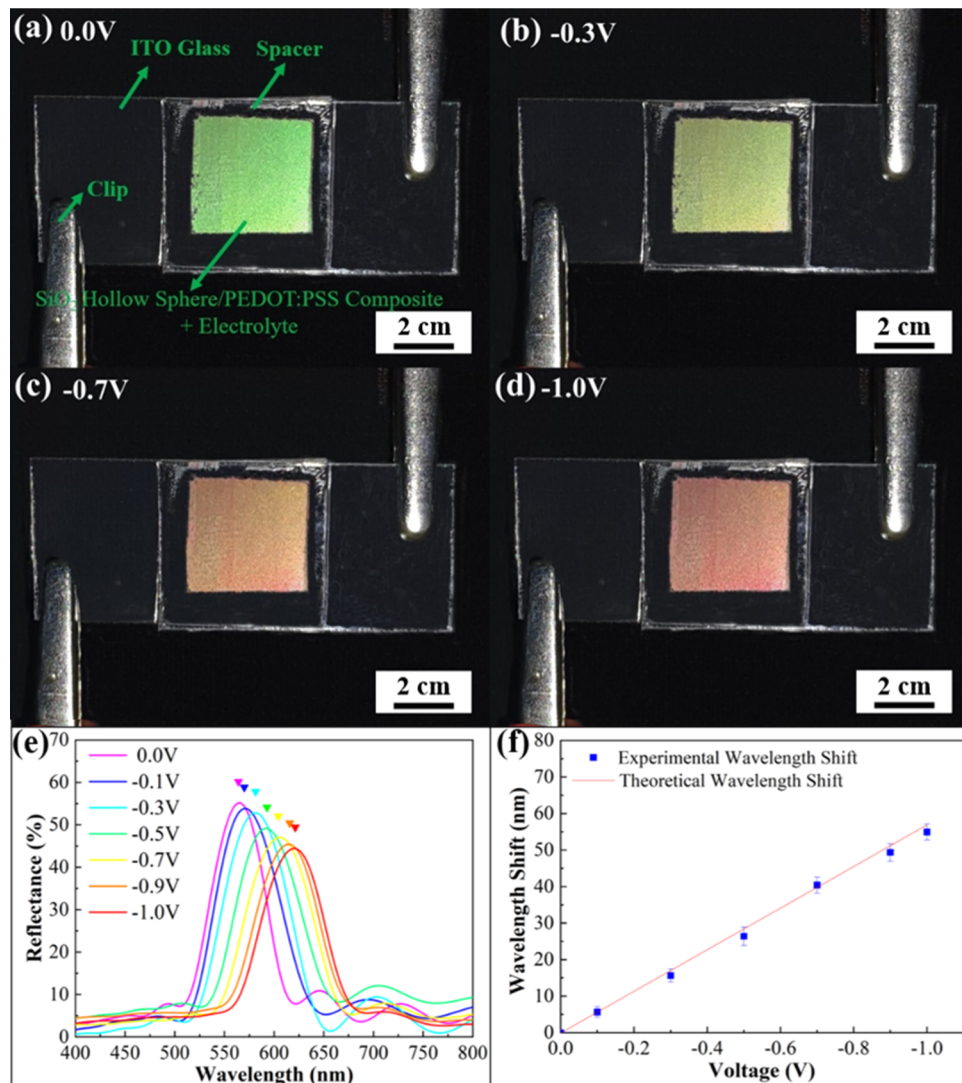


**Figure 3.** Color change of an electrochromic device composed of the 240 nm silica hollow sphere/PEDOT:PSS photonic crystals. Sequential images of the photonic crystals show the expression of varied voltages, (a) 0.0 V, (b) -0.3 V, (c) -0.7 V, and (d) -1.0 V, into visible color changes. (e) Normal-incidence reflection spectra of the photonic crystals under varied voltages. (f) Reflection peak position shift of the photonic crystals versus the applied voltage.

(lithium perchlorate/propylene carbonate = 1:100 by weight) is brush-coated on the photonic crystals, followed by placing another ITO coating glass on the top to build an electrochromic device.<sup>47</sup> For the device, a 25  $\mu\text{m}$  Surlyn hot-melt sealing spacer (The Dow Chemical Co.) is adopted to ensure perfect confinement of the electrolyte after hot press lamination. The electrical actuation of the photonic crystals is enabled by a DPS-10005 DC power supply (Hila International Inc., Taiwan).

**Characterizations.** Digital photographs of the photonic crystals and the electrochromic device are obtained with a Canon SX720 camera (Canon Inc., Japan). Surface morphologies of the specimens are determined using a JEOL 6335F scanning electron microscope (JEOL Ltd., Japan) after sputter-coating with platinum. Normal-incidence reflection spectra of the specimens are acquired by an Ocean Optics HR4000 fiber-coupled UV-vis-NIR spectrometer equipped with an Ocean Optics DT-MINI-2 power source and recorded through Ocean Optics Spectroscopy Software (Ocean Optics Inc.).

## RESULTS AND DISCUSSION

Inspired by the natural responsive photonic crystals of cephalopods, electrically responsive silica hollow sphere/PEDOT:PSS photonic crystals are engineered in a scalable doctor-blade coating process (Figure 1). First, monodisperse silica hollow spheres with a diameter of 240 nm and an average wall thickness of 18 nm are fabricated and dispersed in a commercial PEDOT:PSS solution, where the volume ratio of silica spheres to PEDOT:PSS copolymer is adjusted to 74:26 (Figure S1). The as-prepared suspension is then deposited and doctor-blade-coated onto an ITO-coated glass, during which the blade renders one-dimensional shear force for aligning the silica hollow spheres. The shear-induced colloidal crystallization is attributed to the shear-thinning behavior of the silica sphere dispersion.<sup>48,49</sup> As a critical shear rate is reached, silica hollow spheres are arranged into layers and glided over each other to reduce their relative viscosity. This further leads to the formation of close-packed colloidal crystals. It is also worth noting that the thickness of doctor-blade-coated photonic crystals is dependent on the rheological properties of

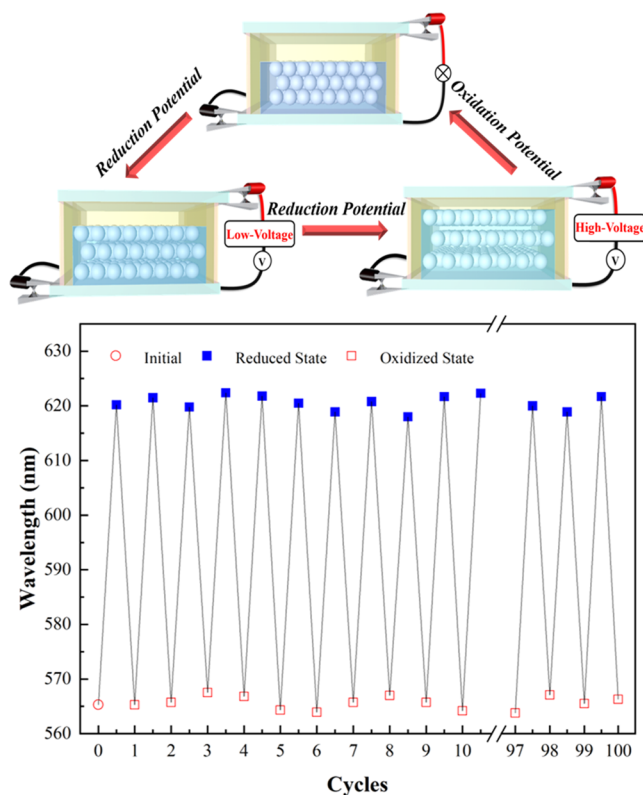


**Figure 4.** Illustration of the concept of cephalopod-inspired color change enabled by electrically responsive photonic crystals. Reversible reflection peak position shift of the electrically responsive photonic crystals between the oxidized state (blue squares) and the reduced state ( $-1.0\text{ V}$ ; red squares) for 100 cycles.

dispersion, the coating speed, the gap size, and the wetting behavior of the substrate.<sup>50,51</sup> After evaporation of any residual water, the self-assembled silica hollow spheres are embedded in

a PEDOT:PSS matrix, which is eventually applied to assemble an electrochromic device.

The resulting 240 nm silica hollow sphere/PEDOT:PSS photonic crystals display a uniform cyan color under white light illumination (Figure 2a). Although a few point vacancies can be found, long-range close-packed silica hollow spheres surrounded by THE PEDOT:PSS matrix are apparent (Figure 2b–d). This sticking color originates from Bragg's diffraction of incident light from the three-dimensional hexagonal crystalline lattice. The crystalline structure and the corresponding optical performance are further evaluated using a fiber-coupled UV-vis-NIR spectrometer. It is noticeable that the measured normal-incidence reflection peak position (499 nm) agrees well with the theoretical one (498 nm) estimated according to Bragg's equation

$$\lambda_{\text{peak}} = 2 \times (n_{\text{air}} \times f_{\text{air}} + n_{\text{silica}} \times f_{\text{silica}} + n_{\text{PEDOT:PSS}} \times f_{\text{PEDOT:PSS}}) \times d \times \sin 90^\circ$$

where  $n_s$ ,  $f_s$ , and  $d$  denote the refractive index, volume fraction, and lattice spacing, respectively (Figure S2).<sup>52</sup> The remarkable agreement once again demonstrates the highly crystalline quality of the doctor-blade-coated photonic crystals. Importantly, in comparison to silica solid sphere/polymer composites, a larger refractive index difference between  $n_{\text{silica hollow sphere}}$  (1.17) and  $n_{\text{PEDOT:PSS}}$  (1.5) leads to a higher reflection intensity.<sup>53</sup>

To characterize electrochromic characteristics of silica hollow sphere/PEDOT:PSS photonic crystals, the as-engineered photonic crystals are coated with a transparent lithium perchlorate/propylene carbonate electrolyte and then connected to a DC power supply. As would be expected, the corresponding structural color rapidly turns green due to electrolyte swelling (Figure 3a). Electrolyte influx into the PEDOT:PSS copolymer matrix creates an expansion in the crystal lattice and hence leads to a color change. Importantly, the lattice increase takes place primarily perpendicular to the

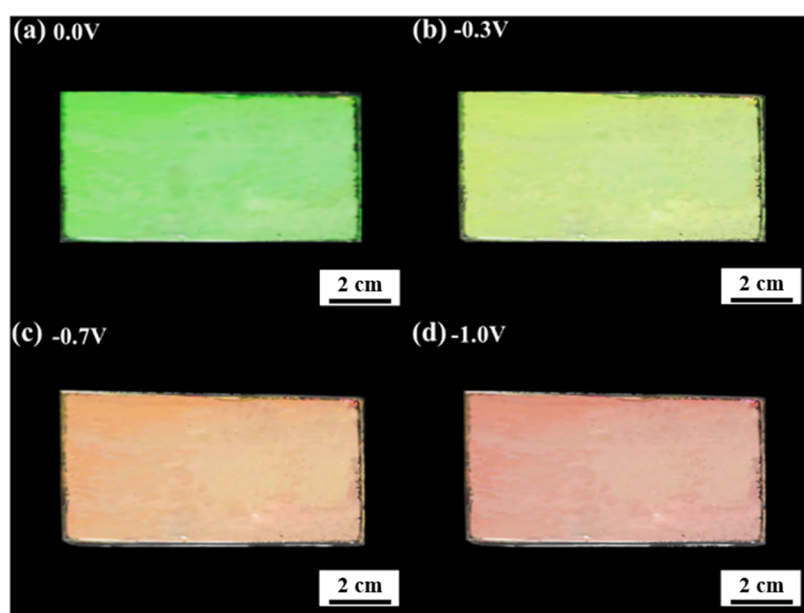


**Figure 5.** Photographic images of the 240 nm silica hollow sphere/PEDOT:PSS photonic crystals after withdrawing from the devices for 24 h. Varied voltages, (a) 0.0 V, (b)  $-0.3\text{ V}$ , (c)  $-0.7\text{ V}$ , and (d)  $-1.0\text{ V}$ , are applied on the devices.

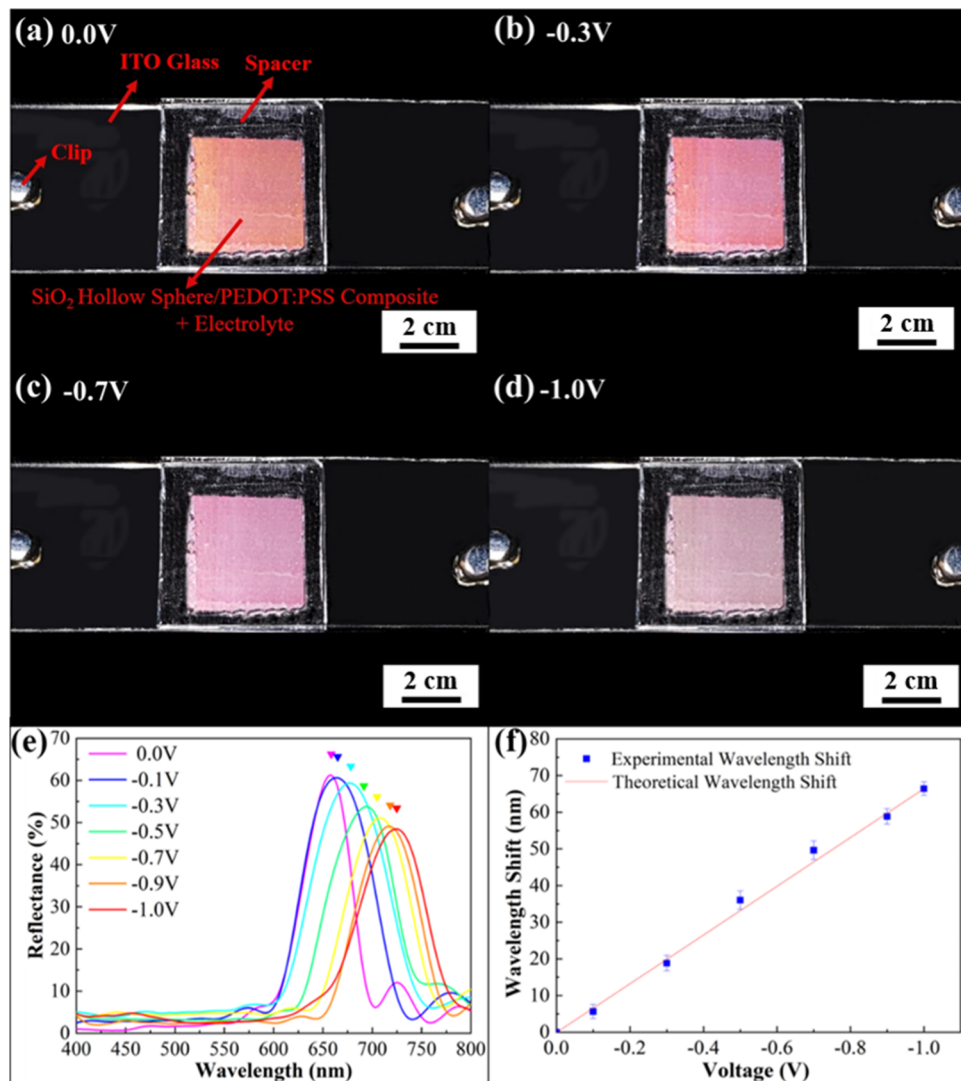


**Figure 6.** Color change of an electrochromic device composed of the 280 nm silica hollow sphere/PEDOT:PSS photonic crystals. Sequential images of the photonic crystals show the expression of varied voltages, (a) 0.0 V, (b) -0.3 V, (c) -0.7 V, and (d) -1.0 V, into visible color changes. (e) Normal-incidence reflection spectra of the photonic crystals under varied voltages. (f) Reflection peak position shift of the photonic crystals versus the applied voltage.

glass substrate on account of the covalent anchoring of the copolymer.<sup>54</sup> Once reduction potentials are applied, electrons are driven into the photonic crystals, while lithium cations accompanied by the electrolyte penetrate into the copolymer matrix to neutralize its negative charge buildup. Further electrolyte swelling pushes apart the silica hollow sphere layers, increasing the interlayer lattice spacing (*d*) and hence red-shifting the resulting band gap position. As a result, the structural color can be easily changed between green (0 V), yellow (-0.3 V), orange (-0.7 V), and red (-1.0 V) by applying various voltages (Figure 3a–d). Importantly, the photonic crystals exhibit uniform colors with high color saturation. Even though unpatterned PEDOT:PSS copolymer films (~10  $\mu\text{m}$  in thickness) are light blue in different electric fields, their low reflectances (~5%) cannot significantly affect the appearances of silica hollow sphere/PEDOT:PSS photonic crystals (Figure S2a). To further comprehend the color changes, normal-incidence reflection spectra of the photonic crystals under varied voltages are compared in Figure 3e. It is worth mentioning that the color change is completed within 1

s after application of a particular voltage, and yet, the spectra are recorded after maintaining the applied voltage for 2 min to ensure that the system reaches an equilibrium. Clearly, the reflection peak incrementally red-shifts when the voltage is gradually varied from 0 to -1.0 V. Although the reflection is slightly reduced due to medium refractive index matching, its intensity can be improved by increasing the silica hollow sphere layers of the photonic crystals. Interestingly, the thickness expansion of the PEDOT:PSS copolymer film is proportional to the voltages on electrolyte swelling (Figure S2b). Owing to the effective refractive index of the photonic crystals almost keeping consistent as the electrolyte influx into the copolymer matrix, the reflection peak position shift is in a nearly linear relationship with the applied voltage (Figure 3f). Notwithstanding the fact that the wavelength shift remains unchanged under an even higher voltage, the ultimate range of dynamic electrochromic tunability can be determined through controlling the interlayer lattice spacing of photonic crystals.

The coloration and patterning on cephalopod skins can be converted on demand to provide a unique camouflage

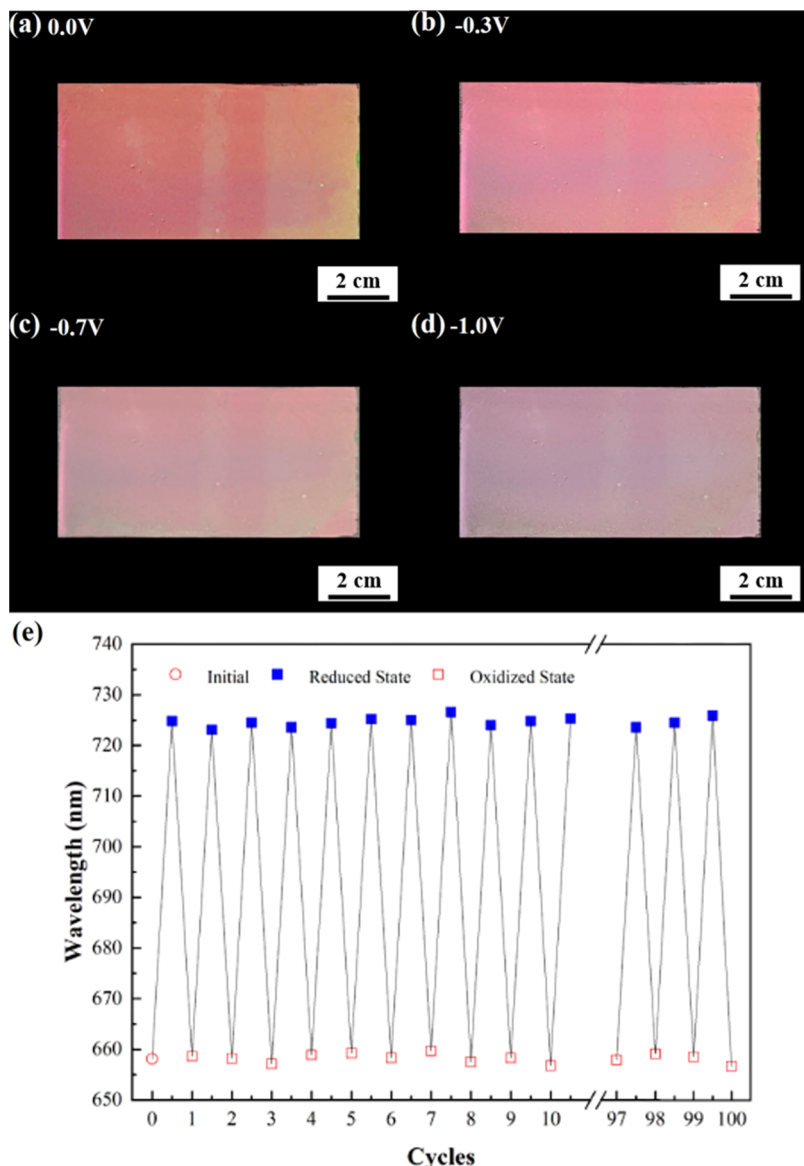


**Figure 7.** Photographic images of the 280 nm silica hollow sphere/PEDOT:PSS photonic crystals after withdrawing from the devices for 24 h. Varied voltages, (a) 0.0 V, (b) -0.3 V, (c) -0.7 V, and (d) -1.0 V, are applied on the devices. (e) Reversible reflection peak position shift of the electrically responsive photonic crystals between the oxidized state (blue squares) and the reduced state (-1.0 V; red circles) for 100 cycles.

capability. Such an extraordinary feature is enabled by repeatedly alternating the geometries and extracellular spaces of innervated protein layers. Similarly, electrochemically driven PEDOT:PSS copolymer matrix swelling and shrinking actively mediate the interlayer lattice spacing of the photonic crystals (Figure 4). The process runs in reverse once applying an oxidation potential, during which electrons and the electrolyte are drawn out of the matrix. Consequently, the photonic crystals recover their original crystalline lattice and intrinsic color. As recognized, the reflection peak position of the recovered photonic crystals matches well with that of the initial one, disclosing that the original lattice spacing is fully recovered. The cycling stability of the electrically responsive photonic crystals is assessed as well in this study. It is found that the reflection peak position reversibly shifts between 563 and 623 nm after each voltage application for a series of 100 reduction/oxidation cycles without any failure. Importantly, the electrically responsive photonic crystals can keep their temporary structures even without any electric field under

ambient conditions. Thanks to the low vapor pressure of the electrolyte, the photonic crystals are capable of maintaining their striking colors for at least 24 h after withdrawing from the devices (Figure 5).<sup>55</sup> It is worth noting that the structural color can be preserved, while the reflectance is decreased by less than 5% after 100 reduction/oxidation cycles (Figure S4). The highly reversible and stable electrochromism for a wide range of colors is even comparable with most electrochromic materials.<sup>56–58</sup>

The accessible color tuning range of the electrically responsive photonic crystals majorly depends on the starting particle size. To gain a better understanding, 280 nm silica hollow spheres with an average wall thickness of 15 nm are produced and employed to engineer silica hollow sphere/PEDOT:PSS photonic crystals (Figure S5). The as-fabricated photonic crystals display a brilliant green color with high color saturation, which is derived from Bragg's diffraction of visible light by the three-dimensionally close-packed silica hollow spheres (Figure S6). The highly ordered crystalline lattice is

further evidenced via a great consistency between its reflection peak position (567 nm) and a theoretical one (566 nm) (**Figure S7**). As mentioned above, the structural color turns to scarlet and then gradually to red upon applying reduction potentials as a result of electrolyte swelling (**Figure 6a–d**). Anticipatedly, the thickness expansion of the PEDOT:PSS matrix is proportional to the voltages. The corresponding normal-incidence reflection peak position therefore shifts linearly from 660 to 727 nm with the applied voltage (**Figure 6e,f**). Manifestly, this red shift (67 nm) is larger than that (55 nm) of the 240 nm silica hollow sphere/PEDOT:PSS photonic crystals, indicating that larger silica hollow spheres can bring about larger red shifts. This finding further implies that it is valid to develop a full-color display by appropriately selecting the sphere size and thickness. It is noteworthy that the expanded interlayer lattice spacings and the related structural colors are well preserved after disconnecting a power supply for more than 24 h (**Figure 7a–d**). Its original interlayer lattice spacing can then be fully recovered in a few seconds by applying an oxidation potential to pull out the electrolyte. As demonstrated, the lattice spacing and the resulting reflection peak position can be reversibly switched for 100 cycles on demand (**Figure 7e**). Compared with macroporous photonic crystals, hollow sphere-based photonic crystals exhibit greater mechanical properties, which is critical for developing electrochromic displays.

## CONCLUSIONS

By drawing inspiration from cephalopod skins, we develop a roll-to-roll compatible doctor-blade coating technique to self-assemble electrically responsive photonic crystals, wherein close-packed nanometer-sized silica hollow spheres are embedded in an electrically responsive copolymer matrix. Upon applying varied voltages, the interlayer lattice spacing of the photonic crystals can be altered on demand as the innervated protein layers within the cephalopod skin do. In comparison with fragile macroporous photonic crystals, the swelling of nanometer-sized hollow sphere-based photonic crystals with a nonvolatile electrolyte enables reversible color shifts for more than 100 cycles and even maintains a high color saturation under ambient conditions after disconnecting a power supply. Importantly, the introduction of larger silica hollow spheres can bring about larger color shifts, indicating that it is valid to develop a full-color display by appropriately selecting the sphere size and thickness. Such cephalopod-inspired electrochromic photonic crystals are promising for many optical applications.

## ASSOCIATED CONTENT

### Supporting Information

The Supporting Information is available free of charge at <https://pubs.acs.org/doi/10.1021/acsanm.2c03931>.

SEM images and TEM images of silica hollow spheres and photographic images, SEM images, normal-incidence reflection spectra, and the thickness expansion versus the applied voltage of silica hollow sphere/PEDOT:PSS photonic crystals ([PDF](#))

## AUTHOR INFORMATION

### Corresponding Authors

Hui-Ping Tsai – Department of Civil Engineering and Innovation and Development Center of Sustainable

Agriculture, National Chung Hsing University, Taichung City 40227, Taiwan; Email: [huiping.tsai@nchu.edu.tw](mailto:huiping.tsai@nchu.edu.tw)  
Hongta Yang – Department of Chemical Engineering, National Chung Hsing University, Taichung City 40227, Taiwan;  [orcid.org/0000-0002-5822-1469](https://orcid.org/0000-0002-5822-1469); Email: [hyang@dragon.nchu.edu.tw](mailto:hyang@dragon.nchu.edu.tw)

### Authors

Chia-Hua Hsieh – Department of Chemical Engineering, National Chung Hsing University, Taichung City 40227, Taiwan

Fang-Tzu Lin – Department of Chemical Engineering, National Chung Hsing University, Taichung City 40227, Taiwan

Kun-Yi Andrew Lin – Department of Environmental Engineering, National Chung Hsing University, Taichung City 40227, Taiwan

Shang-Yu Hsieh – Department of Chemical Engineering, National Chung Hsing University, Taichung City 40227, Taiwan

Yi-Ting Chen – Department of Chemical Engineering, National Chung Hsing University, Taichung City 40227, Taiwan

Chieh-Hsuan Lu – Department of Chemical Engineering, National Chung Hsing University, Taichung City 40227, Taiwan

Complete contact information is available at:  
<https://pubs.acs.org/10.1021/acsanm.2c03931>

### Notes

The authors declare no competing financial interest.

## ACKNOWLEDGMENTS

Acknowledges are made to the National Science Council (110-2221-E-005-050-MY2, 111-2221-E-005-010, and 111-2121-M-005-002) and the Innovation and Development Center of Sustainable Agriculture from The Featured Areas Research Center Program within the framework of the Higher Education Sprout Project by the Ministry of Education for financial support. Additionally, the authors acknowledge the technical support with the field-emission scanning electron microscope from the Instrument Center of the National Chung Hsing University.

## REFERENCES

- (1) Kirillova, A.; Marschelke, C.; Synytska, A. Hybrid Janus Particles: Challenges and Opportunities for the Design of Active Functional Interfaces and Surfaces. *ACS Appl. Mater. Interfaces* **2019**, *11*, 9643–9671.
- (2) Nam, S. K.; Kim, J. B.; Han, S. H.; Kim, S. H. Photonic Janus Balls with Controlled Magnetic Moment and Density Asymmetry. *ACS Nano* **2020**, *14*, 15714–15722.
- (3) Xie, S. T.; Ai, L. L.; Cui, C.; Fu, T.; Cheng, X. D.; Qu, F. L.; Tan, W. H. Functional Aptamer-Embedded Nanomaterials for Diagnostics and Therapeutics. *ACS Appl. Mater. Interfaces* **2021**, *13*, 9542–9560.
- (4) Lu, Y. S.; Vijayakumar, S.; Chaix, A.; Pimentel, B. R.; Bentz, K. C.; Li, S.; Chan, A.; Wahl, C.; Ha, J. S.; Hunka, D. E.; Boss, G. R.; Cohen, S. M.; Sailor, M. J. Remote Detection of HCN, HF, and Nerve Agent Vapors Based on Self-Referencing, Dye-Impregnated Porous Silicon Photonic Crystals. *ACS Sens.* **2021**, *6*, 418–428.
- (5) Hussain, S.; Park, S. Y. Sweat-Based Noninvasive Skin-Patchable Urea Biosensors with Photonic Interpenetrating Polymer Network Films Integrated into PDMS Chips. *ACS Sens.* **2020**, *5*, 3988–3998.

- (6) Saraswat, Y. C.; Ibis, F.; Rossi, L.; Sasso, L.; Eral, H. B.; Fanzio, P. Shape Anisotropic Colloidal Particle Fabrication using 2-Photon Polymerization. *J. Colloid Interface Sci.* **2020**, *564*, 43–51.
- (7) Abumelha, H. M.; Hameed, A.; Alkhamis, K. M.; Alkabli, J.; Aljuhani, E.; Shah, R.; El-Metwaly, N. M. Development of Mechanically Reliable and Transparent Photochromic Film Using Solution Blowing Spinning Technology for Anti-Counterfeiting Applications. *ACS Omega* **2021**, *6*, 27315–27324.
- (8) Shi, C.; Shen, X. Y.; Zhu, Y. N.; Li, X. Q.; Pang, Z. Y.; Ge, M. Q.; Abolhasani, M. Facile Synthesis of a Color-Tunable Microcrystal Phosphor for Anti-Counterfeit Applications. *ACS Omega* **2020**, *5*, 32420–32425.
- (9) Dong, Y. X.; Bazrafshan, A.; Pokutta, A.; Sulejmani, F.; Sun, W.; Combs, J. D.; Clarke, K. C.; Salaita, K. Chameleon-Inspired Strain-Accommodating Smart Skin. *ACS Nano* **2019**, *13*, 9918–9926.
- (10) Fu, Y.; Wang, Y. M.; Chen, D.; Yu, Z. H.; Zheng, J. Q.; Zhou, H. M. Three-Dimensional Photonic Crystal Bulks with Outstanding Mechanical Performance Assembled by Thermoforming-Etching Cross-linked Polymer Microspheres. *ACS Appl. Mater. Interfaces* **2020**, *12*, 35311–35317.
- (11) Xu, J.; Zhang, B. B.; Jia, L.; Fan, Y. P.; Chen, R. J.; Zhu, T. H.; Liu, B. Z. Dual-Mode, Color-Tunable, Lanthanide-Doped Core-Shell Nanoarchitectures for Anti-Counterfeiting Inks and Latent Fingerprint Recognition. *ACS Appl. Mater. Interfaces* **2019**, *11*, 35294–35304.
- (12) Jaiswal, A. K.; Hokkanen, A.; Kumar, V.; Makela, T.; Harlin, A.; Orelma, H. Thermoresponsive Nanocellulose Films as an Optical Modulation Device: Proof-of-Concept. *ACS Appl. Mater. Interfaces* **2021**, *13*, 25346–25356.
- (13) Bruzas, I.; Brinson, B. E.; Gorunmez, Z.; Lum, W.; Ringe, E.; Sagle, L. Surface-Enhanced Raman Spectroscopy of Fluid-Supported Lipid Bilayers. *ACS Appl. Mater. Interfaces* **2019**, *11*, 33442–33451.
- (14) Pushina, M.; Penavic, A.; Farshbaf, S.; Anzenbacher, P. Fluorescent Sensor Array for Quantitative Determination of Saccharides. *ACS Sens.* **2021**, *6*, 4001–4008.
- (15) Xu, C.; Liu, Y.; Xiong, T. Y.; Wu, F.; Yu, P.; Wang, J. H.; Mao, L. Q. Dynamic Behavior of Charged Particles at the Nanopipette Orifice. *ACS Sens.* **2021**, *6*, 2330–2338.
- (16) Tsutsui, M.; Yokota, K.; He, Y. H.; Washio, T.; Kawai, T. Nano-corrugated Nanochannels for In Situ Tracking of Single-Nanoparticle Translocation Dynamics. *ACS Sens.* **2020**, *5*, 2530–2536.
- (17) Lequieu, J.; Quah, T.; Delaney, K. T.; Fredrickson, G. H. Complete Photonic Band Gaps with Nonfrustrated ABC Bottlebrush Block Polymers. *ACS Macro Lett.* **2020**, *9*, 1074–1080.
- (18) Lei, Q. L.; Ni, R.; Ma, Y. Q. Self-Assembled Chiral Photonic Crystals from a Colloidal Helix Racemate. *ACS Nano* **2018**, *12*, 6860–6870.
- (19) Seo, S. E.; Girard, M.; de la Cruz, M. O.; Mirkin, C. A. The Importance of Salt-Enhanced Electrostatic Repulsion in Colloidal Crystal Engineering with DNA. *ACS Cent. Sci.* **2019**, *5*, 186–191.
- (20) Kamysbayev, V.; Srivastava, V.; Ludwig, N. B.; Borkiewicz, O. J.; Zhang, H.; Ilavsky, J.; Lee, B.; Chapman, K. W.; Vaikuntanathan, S.; Talapin, D. V. Nanocrystals in Molten Salts and Ionic Liquids: Experimental Observation of Ionic Correlations Extending beyond the Debye Length. *ACS Nano* **2019**, *13*, 5760–5770.
- (21) Kwizera, E. A.; Sun, M. R.; White, A. M.; Li, J. R.; He, X. M. Methods of Generating Dielectrophoretic Force for Microfluidic Manipulation of Bioparticles. *ACS Biomater. Sci. Eng.* **2021**, *7*, 2043–2063.
- (22) Lim, S. Y.; Hedrich, C.; Jiang, L.; Law, C. S.; Chirumamilla, M.; Abell, A. D.; Blick, R. H.; Zierold, R.; Santos, A. Harnessing Slow Light in Optoelectronically Engineered Nanoporous Photonic Crystals for Visible Light-Enhanced Photocatalysis. *ACS Catal.* **2021**, *11*, 12947–12962.
- (23) Xu, X.; Franke, T.; Schilling, K.; Sommerdijk, N.; Colfen, H. Binary Colloidal Nanoparticle Concentration Gradients in a Centrifugal Field at High Concentration. *Nano Lett.* **2019**, *19*, 1136–1142.
- (24) An, S. G.; Gao, L.; Hao, A. Y.; Xing, P. Y. Ultraviolet Light Detectable Circularly Polarized Room Temperature Phosphorescence in Chiral Naphthalimide Self-Assemblies. *ACS Nano* **2021**, *15*, 20192–20202.
- (25) Qi, F. L.; Meng, Z. H.; Xue, M.; Qiu, L. L. Recent Advances in Self-Assemblies and Sensing Applications of Colloidal Photonic Crystals. *Anal. Chim. Acta* **2020**, *1123*, 91–112.
- (26) Wang, J.; Pinkse, P. W. H.; Segerink, L. I.; Eijkel, J. C. T. Bottom-Up Assembled Photonic Crystals for Structure-Enabled Label-Free Sensing. *ACS Nano* **2021**, *15*, 9299–9327.
- (27) Zhang, Z. J.; Qi, Y.; Ma, W.; Zhang, S. F. Wettability-Controlled Directional Actuating Strategy Based on Bilayer Photonic Crystals. *ACS Appl. Mater. Interfaces* **2021**, *13*, 2007–2017.
- (28) Chen, K.; Fu, Q. Q.; Ye, S. Y.; Ge, J. P. Multicolor Printing Using Electric-Field-Responsive and Photocurable Photonic Crystals. *Adv. Funct. Mater.* **2017**, *27*, No. 1702825.
- (29) Yue, Y. F.; Norikane, Y.; Gong, J. P. Ultrahigh-Water-Content Photonic Hydrogels with Large Electro-Optic Responses in Visible to Near-Infrared Region. *Adv. Opt. Mater.* **2021**, *9*, No. 2002198.
- (30) Zhang, Z. H.; Chen, Z. Y.; Wang, Y.; Zhao, Y. J. Bioinspired Conductive Cellulose Liquid-Crystal Hydrogels as Multifunctional Electrical Skins. *Proc. Natl. Acad. Sci. U.S.A.* **2020**, *117*, 18310–18316.
- (31) Shen, Q. C.; Ma, S.; Luo, Z.; An, S.; He, J. Q.; Zhang, R. X.; Tao, P.; Song, C. Y.; Wu, J. B.; Potyrailo, R. A.; Deng, T.; Shang, W. Butterfly Wing Inspired High-Performance Infrared Detection with Spectral Selectivity. *Adv. Opt. Mater.* **2020**, *8*, No. 1901647.
- (32) Bouchal, P.; Kapitan, J.; Konecny, M.; Zboncak, M.; Bouchal, Z. Non-Diffracting Light in nature: Anomalously Reflected Self-Healing Bessel Beams from Jewel Scarabs. *APL Photonics* **2019**, *4*, No. 126102.
- (33) Xu, C. Y.; Stiubianu, G. T.; Gorodetsky, A. A. Adaptive Infrared-Reflecting Systems Inspired by Cephalopods. *Science* **2018**, *359*, 1495–1500.
- (34) Deravi, L. F.; Magyar, A. P.; Sheehy, S. P.; Bell, G. R. R.; Mathger, L. M.; Senft, S. L.; Wardill, T. J.; Lane, W. S.; Kuzirian, A. M.; Hanlon, R. T.; Hu, E. L.; Parker, K. K. The Structure-Function Relationships of a Natural Nanoscale Photonic Device in Cuttlefish Chromatophores. *J. R. Soc., Interface* **2014**, *11*, No. 20130942.
- (35) Walish, J. J.; Kang, Y.; Mickiewicz, R. A.; Thomas, E. L. Bioinspired Electrochemically Tunable Block Copolymer Full Color Pixels. *Adv. Mater.* **2009**, *21*, 3078.
- (36) Vaezi, M.; Seitz, H.; Yang, S. F. A Review on 3D Micro-Additive Manufacturing Technologies. *Int. J. Adv. Manuf. Technol.* **2013**, *67*, 1721–1754.
- (37) Lee, H. S.; Shim, T. S.; Hwang, H.; Yang, S. M.; Kim, S. H. Colloidal Photonic Crystals toward Structural Color Palettes for Security Materials. *Chem. Mater.* **2013**, *25*, 2684–2690.
- (38) Lavorato, G. C.; Das, R.; Xing, Y. T.; Robles, J.; Litterst, F. J.; Saitovitch, E. B.; Phan, M. H.; Srikanth, H. Origin and Shell-Driven Optimization of the Heating Power in Core/Shell Bimagnetic Nanoparticles. *ACS Appl. Nano Mater.* **2020**, *3*, 1755.
- (39) Hsieh, C. H.; Lu, Y. C.; Yang, H. T. Self-Assembled Mechanochromic Shape Memory Photonic Crystals by Doctor Blade Coating. *ACS Appl. Mater. Interfaces* **2020**, *12*, 36478–36484.
- (40) Cao, X.; Pan, G. S.; Huang, P.; Guo, D.; Xie, G. X. Silica-Coated Core-Shell Structured Polystyrene Nanospheres and Their Size-Dependent Mechanical Properties. *Langmuir* **2017**, *33*, 8225–8232.
- (41) Sarma, D.; Carl, P.; Climent, E.; Schneider, R. J.; Rurack, K. Multifunctional Polystyrene Core/Silica Shell Microparticles with Antifouling Properties for Bead-Based Multiplexed and Quantitative Analysis (vol 11, pg 1321, 2019). *ACS Appl. Mater. Interfaces* **2019**, *11*, 11028.
- (42) Yu, J.; Yan, Q. F.; Shen, D. Z. Co-Self-Assembly of Binary Colloidal Crystals at the Air-Water Interface. *ACS Appl. Mater. Interfaces* **2010**, *2*, 1922–1926.
- (43) Stöber, W.; Fink, A.; Bohn, E. Controlled Growth of Monodisperse Silica Spheres in the Micron Size Range. *J. Colloid Interface Sci.* **1968**, *26*, 62–69.

- (44) Khanal, A.; Inoue, Y.; Yada, M.; Nakashima, K. Synthesis of Silica Hollow Nanoparticles Templatized by Polymeric Micelle with Core-Shell-Corona Structure. *J. Am. Chem. Soc.* **2007**, *129*, 1534.
- (45) Zhang, L.; D'Acunzi, M.; Kapple, M.; Auernhammer, G. K.; Volmer, D.; van Kats, C. M.; van Blaaderen, A. Hollow Silica Spheres: Synthesis and Mechanical Properties. *Langmuir* **2009**, *25*, 2711–2717.
- (46) Yang, M.; Wang, G.; Yang, Z. Z. Synthesis of Hollow Spheres with Mesoporous Silica Nanoparticles Shell. *Mater. Chem. Phys.* **2008**, *111*, 5–8.
- (47) Argun, A. A.; Cirpan, A.; Reynolds, J. R. The First Truly All-Polymer Electrochromic Devices. *Adv. Mater.* **2003**, *15*, 1338.
- (48) Dong, S.; Zhang, K.; Liu, X.; Yin, Q.; Yip, H. L.; Huang, F.; Cao, Y. Efficient Organic-Inorganic Hybrid Cathode Interfacial Layer Enabled by Polymeric Dopant and its Application in Large-Area Polymer Solar Cells. *Sci. China: Chem.* **2019**, *62*, 67–73.
- (49) Jewloszewicz, B.; Bogdanowicz, K. A.; Przybyl, W.; Iwan, A.; Plebankiewicz, I. PEDOT:PSS in Water and Toluene for Organic Devices—Technical Approach. *Polymers* **2020**, *12*, No. 565.
- (50) Yang, H. T.; Jiang, P. Large-Scale Colloidal Self-Assembly by Doctor Blade Coating. *Langmuir* **2010**, *26*, 13173–13182.
- (51) Padmanabhan, S. C.; McGrath, J.; Bardosova, M.; Pemble, M. E. A Facile Method for the Synthesis of Highly Monodisperse Silica@Gold@Silica Core-Shell-Shell Particles and their use in the Fabrication of Three-Dimensional Metallo dielectric Photonic Crystals. *J. Mater. Chem.* **2012**, *22*, 11978–11987.
- (52) Boilard, T.; Bilodeau, G.; Morency, S.; Messaddeq, Y.; Fortier, R.; Trepanier, F.; Bernier, M. Curvature Sensing using a Hybrid Polycarbonate-Silica Multicore Fiber. *Opt. Express* **2020**, *28*, 39387–39399.
- (53) Salcedo-Reyes, J. C.; Vasquez-Rojas, J. R.; Jimenez-Borrego, L. C.; Castaneda-Uribe, O. A.; Mendez-Pinzon, H. A. Improving Extraction Efficiency of OLEDs by a Luminescent Polymer Embedded in a Colloidal Crystal Matrix. *Semicond. Sci. Technol.* **2019**, *34*, No. 115016.
- (54) Arsenault, A. C.; Kitaev, V.; Manners, I.; Ozin, G. A.; Mihi, A.; Miguez, H. Vapor Swellable Colloidal Photonic Crystals with Pressure Tunability. *J. Mater. Chem.* **2005**, *15*, 133–138.
- (55) Wang, H.; Zhang, K. Q. Photonic Crystal Structures with Tunable Structure Color as Colorimetric Sensors. *Sensors* **2013**, *13*, 4192–4213.
- (56) Jiang, S. A.; Chang, J. L.; Lin, J. W.; Zhang, Y. S.; Mo, T. S.; Lin, J. D.; Lee, C. R. Toward Full-Color Tunable Chiroptical Electro-thermochromic Devices Based on a Supramolecular Chiral Photonic Material. *Adv. Opt. Mater.* **2021**, *9*, No. 2001796.
- (57) Radka, B. P.; King, B. E.; McConney, M. E.; White, T. J. Electrically Induced Splitting of the Selective Reflection in Polymer Stabilized Cholesteric Liquid Crystals. *Adv. Opt. Mater.* **2020**, *8*, No. 2000914.
- (58) Song, G. Y.; Oh, C.; Sinha, S.; Son, J.; Heo, J. Facile Phase Control of Multivalent Vanadium Oxide Thin Films (V<sub>2</sub>O<sub>5</sub> and VO<sub>2</sub>) by Atomic Layer Deposition and Postdeposition Annealing. *ACS Appl. Mater. Interfaces* **2017**, *9*, 23909–23917.

## □ Recommended by ACS

### Heterogeneous Self-Assembly of a Single Type of Nanoparticle Modulated by Skin Formation

Chang Li, Ho Cheung Shum, et al.  
JUNE 12, 2023  
ACS NANO

READ ▾

### Centrifugation-Assisted Growth of Single-Crystalline Grains in Microcapsules

Young Geon Kim, Shin-Hyun Kim, et al.  
JANUARY 17, 2023  
ACS NANO

READ ▾

### Micropatterning of Quantum Dots for Biofunctionalization and Nanoimaging

Paul Robineau, Cyrille Vézy, et al.  
MAY 08, 2023  
ACS APPLIED NANO MATERIALS

READ ▾

### 3D Optical Heterostructure Patterning by Spatially Allocating Nanoblocks on a Printed Matrix

Kaixuan Li, Yanlin Song, et al.  
SEPTEMBER 12, 2022  
ACS NANO

READ ▾

Get More Suggestions >